Structural variations of amorphous magnesium carbonate during nucleation, crystallization, and decomposition of nesquehonite $MgCO_3 \cdot 3H_2O$

Gen-ichiro Yamamoto, Atsushi Kyono*, Satoru Okada

Division of Earth Evolution Sciences, Graduate School of Life and Environmental Sciences, University of Tsukuba, 1-1-1 Tennodai, Tsukuba, 305-8572, Japan

**Corresponding author: kyono@geol.tsukuba.ac.jp,* ORCiD: 0000-0001-5419-390X

Abstract

Carbonate minerals are major contributors to carbon sequestration in geological deposits; however, their nature and behavior remain unclear. Amorphous magnesium carbonate (AMC) is formed as a precursor to crystalline magnesium carbonates and as a product of thermal decomposition of nesquehonite (NSQ). In this study, the AMCs formed during the crystallization and decomposition of NSQ were investigated using X-ray diffraction (XRD) and atomic pair distribution function (PDF) methods. An AMC with a hydromagnesite-like structure (AMC-I) was formed immediately after mixing $MgCl_2$ and Na_2CO_3 solutions. After 5 min of stirring, no change was observed in the XRD pattern; however, the PDF pattern changed. This suggests that the medium-range ordered structure of AMC-I transformed into an intermediate structure (AMC-II) between AMC-I and NSQ. After 10 min of stirring, the AMC-II crystallized into NSQ. In the case of Rb_2CO_3, the AMC-II structure was formed immediately after the mixing of solutions and was stable for three days. AMC-II in the Rb_2CO_3 solution appeared to be in equilibrium with energetic local minima, indicating the existence of polyamorphism in AMC. When Cs_2CO_3 solution was used, the first precipitate had an AMC-I structure. By stirring for 5 min, the AMC-I was transformed to AMC-II, and after 10 min of stirring, a few quantities crystallized into NSQ. After three days, NSQ

dissolved and transformed back into AMC-I. Thus, it is inferred that the crystallization of NSQ is significantly influenced by alkali cations in aqueous solutions. The AMC formed during the thermal decomposition also possesses the AMC-I structure.

Keywords. Amorphous magnesium carbonate, nesquehonite, hydromagnesite, dypingite, atomic pair distribution

Introduction

Carbon capture and storage (CCS) is considered to be one of the most effective technologies for reducing anthropogenic CO_2 emissions (Oelkers et al. 2008; Sanna et al. 2014). In 2012, the UK Department for Energy and Climate Change (DECC) estimated that CCS alone can contribute to 19% of the required global reduction in CO_2 emissions by 2050 (DECC 2012). For this, four main trapping mechanisms have been introduced: stratigraphic (structural), residual, solubility, and mineral (Aminu et al. 2017). Stratigraphic and residual trappings can store CO_2 as a high-density free phase. Solubility trapping allows CO_2 to be stored in its soluble state. Mineral trapping involves geochemical reactions between the injected CO_2 and alkaline minerals in the host rock and leads to the precipitation of carbonate that effectively locks up the CO_2 in the immobile secondary phase in geological timescales (Bachu et al. 1994). The inherent effectivity of mineral trapping by carbonation is evidenced by the fact that >70% of the total carbon in Earth's crust is present in the form of carbonates, of which >90% are calcite ($CaCO_3$) and dolomite ($CaMg(CO_3)_2$) (Hunt 1972; Reeder 1983).

Amorphous calcium carbonate (ACC) and amorphous magnesium carbonate (AMC) are formed as precursors to these crystalline carbonates in aqueous solutions that include metal ions and

(bi)carbonate ions at low temperatures (Rodriguez-Blanco et al. 2011; White et al. 2014; Tobler et al. 2016. Tanaka et al. 2019). However, AMC does not form magnesite ($MgCO_3$) below 120 °C (Di Lorenzo et al. 2014) because of the strong hydration status of the Mg^{2+} ions (Hänchen et al. 2008). Instead, various hydrated magnesium carbonates are formed in aqueous solutions depending on the temperature, partial pressure of CO_2, and pH (Back and Mandarino 2008; Beinlich and Austrheim 2012; Frost et al. 2008; Hänchen et al. 2008; Hopkinson et al. 2012; Kristova et al. 2014; Perchiazzi and Merlino 2006; Tanaka et al. 2019; Yamamoto et al. 2021a, 2021b, 2022).

Recently, it was revealed that AMC possesses the local structure of hydromagnesite (HMG) (Yamamoto et al. 2021c), which is composed of corrugated layers of MgO_6 octahedra and CO_3 groups (Fig. 1a) (Akao and Iwai 1977). AMC precipitates immediately after mixing the $MgCl_2$ and Na_2CO_3 solutions. At temperatures below 55 °C, it subsequently crystallizes into nesquehonite (NSQ) (Kloprogge et al. 2003; Yamamoto et al. 2021b; Zhang et al. 2006), forming one-dimensional infinite ribbons of MgO_6 octahedra and CO_3 groups that extend parallel to the *b*-axis (Fig. 1b) (Giester et al. 2000). They are interconnected by hydrogen bonds of the water molecules between the ribbons. NSQ is eventually transformed into dypingite (DYP) through a solvent-mediated process (Tanaka et al. 2019). DYP also has an HMG-type structure (Hopkinson et al. 2012; Yamamoto et al. 2022). Various carbon sources, such as CO_2 (Ballirano et al. 2010; Ballirano et al, 2013; Hopkinson et al. 2012), Na_2CO_3 (Bhattacharjya et al. 2012; Jauffret et al. 2015; Ren et al. 2014; Tanaka et al. 2019; White et al. 2014; Yamamoto et al. 2021a, 2021b, 2022), K_2CO_3 (Zhang et al. 2006), and $(NH_4)_2CO_3$ (Wang et al. 2008), have been utilized to obtain crystalline magnesium carbonate hydrates. However, few studies have assessed the effects of alkali cations present in aqueous solutions on the crystallization and stability of magnesium carbonate

hydrates. Therefore, in this study, the effects of alkali cations on the nucleation of AMC and crystallization of NSQ were investigated using X-ray diffraction and atomic pair distribution function (PDF) methods. Furthermore, the structure of AMC formed during the thermal decomposition process of NSQ was investigated.

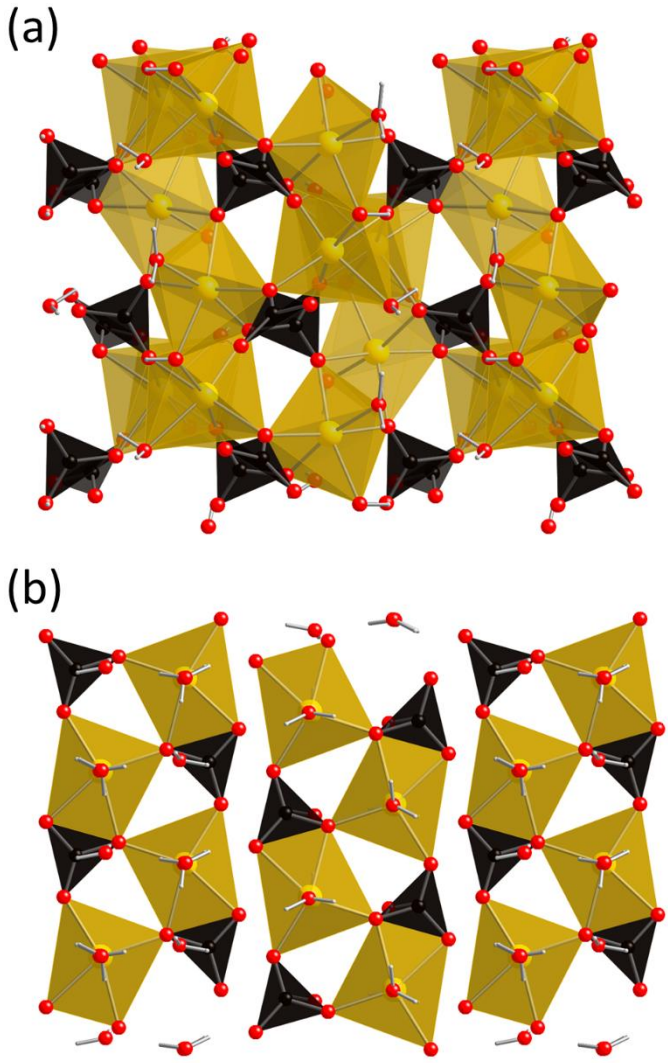

Fig. 1 Crystal structures of (a) hydromagnesite [$Mg_5(CO_3)_4(OH)_2{\cdot}4H_2O$] (Akao and Iwai 1977) and (b) nesquehonite ($MgCO_3{\cdot}3H_2O$) (Giester et al. 2000). Yellow polyhedra and black triangles represent MgO_6 octahedra and CO_3 groups, respectively. Red and small white spheres denote oxygen and hydrogen atoms, respectively

Experimental section

Sample preparation

Commercially available $MgCl_2 \cdot 6H_2O$ (Purity = 98%, FUJIFILM Wako Pure Chemicals Co., Inc., Osaka, Japan), Na_2CO_3 (Purity = 99.8%, FUJIFILM Wako Pure Chemicals Co., Inc., Osaka, Japan) K_2CO_3 (Purity = 99.5%, FUJIFILM Wako Pure Chemicals Co., Inc., Osaka, Japan), Rb_2CO_3 (Purity = 97.0%, FUJIFILM Wako Pure Chemicals Co., Inc., Osaka, Japan), and Cs_2CO_3 (Purity = 95.0%, FUJIFILM Wako Pure Chemicals Co., Inc., Osaka, Japan) were used as starting materials. A 0.5 M aqueous solution of $MgCl_2$ was prepared by adding 50.83 g of $MgCl_2 \cdot 6H_2O$ into a 500 mL beaker containing distilled water. Similarly, 0.5 M Na_2CO_3, K_2CO_3, Rb_2CO_3, and Cs_2CO_3 solutions were prepared by adding 26.50 g of Na_2CO_3, 34.55 g of K_2CO_3, 57.74 g of Rb_2CO_3, and 81.46 g of Cs_2CO_3 into 500 mL beakers containing distilled water, respectively. First, 10 mL of $MgCl_2$ aqueous solution and 10 mL of each alkali carbonic acid solution were mixed at 20 °C in an open system. A white suspension was formed immediately after mixing, which was quickly filtered and washed with distilled water. The samples were air-dried overnight. The obtained sample was denoted as X0min (X indicates the alkali metal in the alkaline carbonate solution). Second, the white suspensions were stirred at ~1,000 rpm for a given time in an open system, after which they were filtered, washed with distilled water, and air-dried overnight. The samples obtained by stirring the white suspension for 5 and 10 min were denoted as X5min and X10min, respectively. The pH of the solutions varied between 10 and 11. Third, the white suspensions were kept under static conditions. After three days, they were filtered, washed with distilled water, and air-dried overnight. The samples were denoted as X3day. The pH of the solutions stabilized at ~10. Furthermore, to investigate the structural characteristics of NSQ during

the thermal decomposition process, the samples of Na10min were heated in an electric furnace to their respective target temperatures. After one hour, they were quickly removed from the furnace and quenched in the air.

Powder X-ray diffraction (XRD) analysis

XRD patterns were recorded using a Bruker D8 Advance diffractometer (Bruker AXS, GmbH, Karlsruhe, Germany) equipped with a position-sensitive LynxEye one-dimensional detector (Bruker AXS, GmbH) using Cu Kα radiation (λ = 1.5418 Å). The powdered sample was spread on a non-reflective Si sample plate. The XRD data were collected in the range of $5° \leq 2\theta \leq 55°$ with a step size of 0.02° and a counting time of 0.3 s per step. The obtained XRD data were analyzed using PDIndexer software (Seto et al. 2010) to calculate the lattice parameters.

Analysis of atomic pair distribution function

Synchrotron X-ray total-scattering measurements were performed at the beamline BL22XU of SPring-8, Japan. Approximately 50 mg of the sample was loaded into a Kapton capillary 15 mm long tube with an inner diameter of 2 mm. The incident beam was monochromatized to a wavelength of 0.206225 Å using a Si (111) double-crystal monochromator. The data were collected in the range of $0.5^o \leq 2\theta \leq 50^o$ corresponding to the Q values, which is defined as $(4\pi\sin\theta)/\lambda$, in the range of 0.3–25 $Å^{-1}$. The 2θ-step increment was 0.01–0.1º depending on the Q value. To obtain sufficient scattering intensity, the measurement time for one sample was approximately 8 h. The obtained X-ray total scattering data were transformed into total scattering structure functions [S(Q)] and atomic PDFs [G(r)] using the PDFgetX2 software (Qiu et al. 2004). The obtained PDF profiles were analyzed using the PDFgui software (Farrow et al. 2007).

Results and discussion

Powder XRD

Na0min exhibited a typical XRD pattern of amorphous materials (Fig. 2a). AMC was the first substance formed by the reaction between $MgCl_2$ and Na_2CO_3. Although Na5min maintained the XRD pattern of AMC, after 10 min of stirring, it showed clear diffraction peaks corresponding to the NSQ. The lattice parameters of NSQ are listed in Table 1. The lattice parameters of Na10min were consistent with those determined in previous studies (Giester et al. 2000; Yamamoto et al. 2021b). The diffraction peaks of NSQ were well maintained after three days. The lattice parameters of Na3day were essentially the same as those of Na10min (Table 1). The magnesium carbonate hydrate formed by mixing $MgCl_2$ and K_2CO_3 solutions exhibited a behavior similar to that obtained from the Na_2CO_3 solution. After stirring for 5 min, several small diffraction peaks of NSQ were observed (Fig. 2b). After 10 min of stirring, the AMC crystallized into NSQ. The diffraction peaks of NSQ were still maintained after three days, but several peaks became distinctly weak, which suggests that the solvent-mediated transformation from NSQ to DYP starts after three days (Tanaka et al. 2019). The lattice parameters of NSQ prepared from both K_2CO_3 and Na_2CO_3 were indistinguishable (Table 1). Therefore, it is inferred that NSQ crystalizes regardless of Na and K cations in the aqueous solutions. The K_2CO_3 solution allows a more rapid crystallization of NSQ compared to the Na_2CO_3 solution.

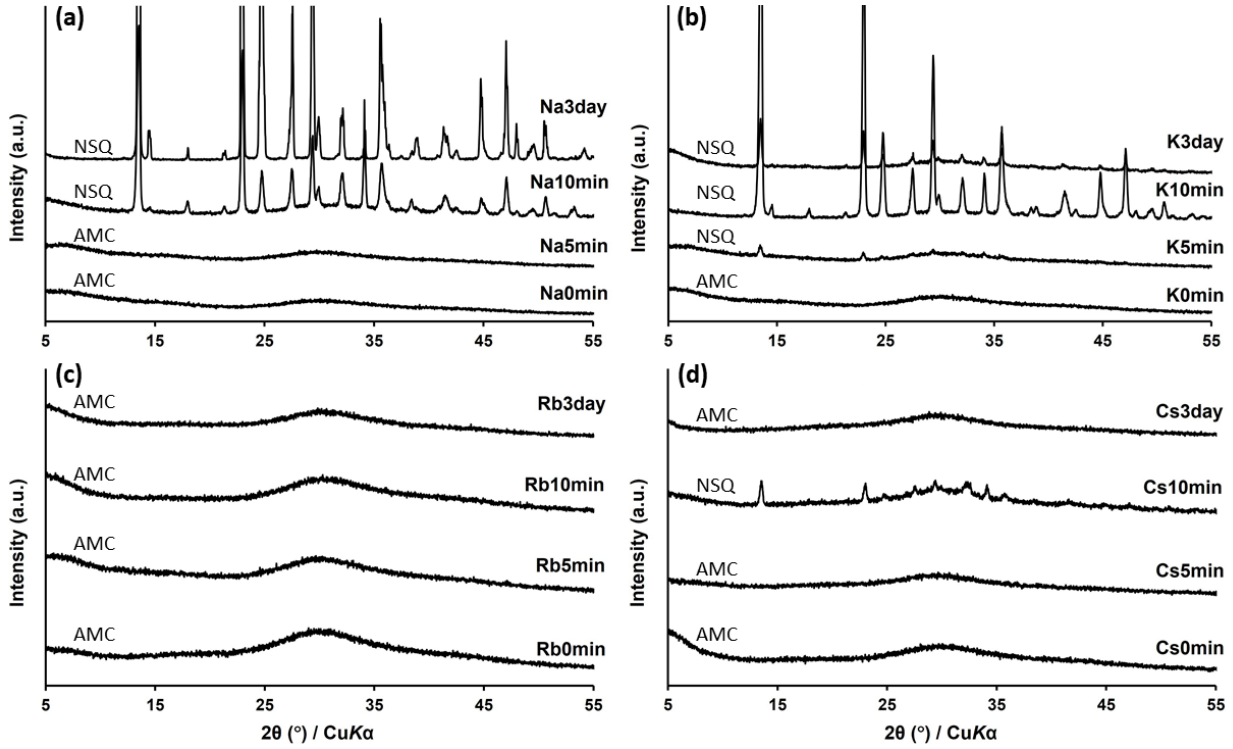

146

147 **Fig. 2** Temporal variation of the X-ray diffraction pattern of amorphous magnesium carbonate
148 (AMC) samples obtained from (a) Na_2CO_3, (b) K_2CO_3, (c) Rb_2CO_3, and (d) Cs_2CO_3 solutions.
149 NSQ: nesquehonite

150

151 However, when Rb_2CO_3 and Cs_2CO_3 solutions were used as carbonate sources, the results were
152 distinctly different from those described above. Rb0min exhibited the typical XRD pattern of
153 AMC (Fig. 2c). Subsequently, NSQ did not crystallize for at least three days. Cs0min and Cs5min
154 also showed the XRD pattern of AMC (Fig. 2d), but Cs10min exhibited weak diffraction peaks of
155 NSQ. Cs3day also exhibited a typical XRD pattern of AMC. It is possible that the NSQ of Cs10min
156 was accidentally formed owing to some unknown reasons. Although the causes of the slight
157 crystallization of Cs10min are unknown, one of the causes might be the crystallization during the
158 filtration process. Thus, it is clear that NSQ crystallization is significantly suppressed by the
159 presence of Rb and Cs cations in aqueous solutions.

Table 1 Lattice parameters of nesquehonite

	a (Å)	*b* (Å)	*c* (Å)	β (°)	V (Å^3)
Na10min	7.724(4)	5.366(1)	12.164(7)	90.03(3)	504.1(6)
Na3day	7.732(5)	5.360(1)	12.161(8)	90.09(3)	504.0(7)
K10min	7.734(7)	5.366(1)	12.160(9)	90.11(5)	504.7(8)
K3day	7.720(6)	5.373(1)	12.167(8)	90.13(5)	504.7(7)

PDF analysis

The atom–pair correlations of Na0min were consistent with those of previously reported AMCs (Jensen et al. 2020; Radha et al. 2012; White et al. 2014; Yamamoto et al. 2021c), in which the characteristic four peaks were observed between 1.0 Å and 4.5 Å (Fig. 3a). The first and second peaks at 1.3 Å and 2.1 Å corresponded to C–O and Mg–O bonds, respectively. The third and fourth peaks at 3.1 Å and 4.2 Å were assigned to Mg–Mg and Mg–O, respectively. This atom–pair correlation pattern was referred to as AMC-I. The atom–pair correlations of Na0min were diminished above 5 Å, which implies that the atomic structure did not possess long-range periodicity. After stirring for 5 min, the third peak of Na5min was split, and a new peak emerged between the third and fourth peaks, although the first and second peaks corresponding to the C–O and Mg–O bonds remained essentially unchanged. This atom–pair correlation pattern observed at Na5min was referred to as AMC-II. In Na5min, the atom–pair correlations above 5 Å were stronger. This suggests that the long-range order in the AMC started to form after 5 min without changing the first coordination spheres around C and Mg atoms. In Na10min, the third peak split at 3.0 and 3.3 Å merged into one peak, although the first and second peaks remained unchanged (Fig. 3a). The atomic–pair correlation peaks above 5 Å became increasingly stronger, which was

probably due to the formation of NSQ. In Na3day, stronger and more evident peaks were observed above 5 Å, suggesting that the degree of NSQ crystallinity increased. Although the first and second atomic–pair correlation peaks corresponding to C–O and Mg–O bonds remained unchanged, the third peak at 3 Å split again. Notably, the atomic–pair correlation peaks from 2.5 Å to 4.5 Å, corresponding to the second coordination spheres, were highly variable between the nucleation of AMC and crystallization of NSQ. A characteristic change could be observed in the range of 2.5–4.5 Å (Fig. 3). Thus, in the PDF pattern of the Na3day, the atomic–pair correlation peaks between 1.0 Å and 6.0 Å were almost identical with those of NSQ obtained by stirring for 2 h (Yamamoto et al. 2021c), except for a split peak at 3.0 Å.

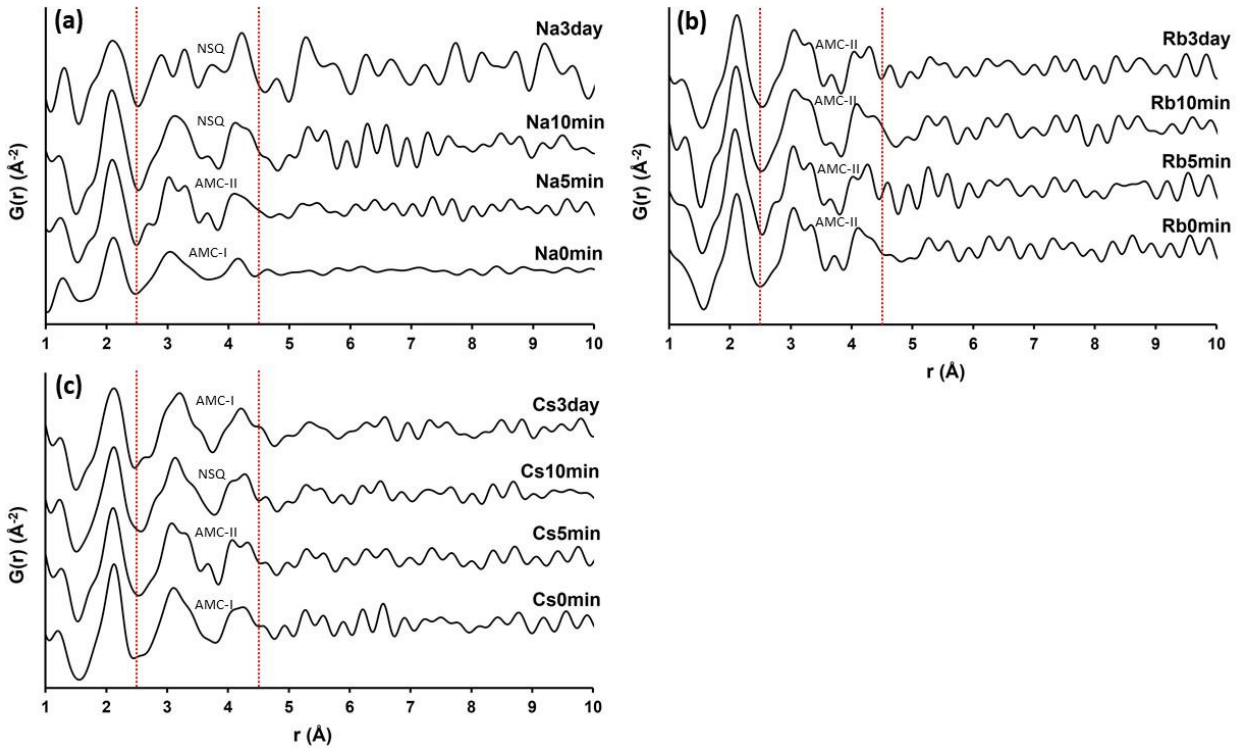

Fig. 3 Time variation of pair distribution function pattern of amorphous magnesium carbonate samples obtained from (a) Na_2CO_3 solution, (b) Rb_2CO_3 solution, and (c) Cs_2CO_3 solution

193 However, when Rb_2CO_3 solution was used as a carbonate source, the medium-range order from
194 1 Å to 10 Å was stable for three days (Fig. 3b), which is one of the most important findings of this
195 study. The medium-range order of the AMC obtained from Rb_2CO_3 solution was different from
196 that of Na0min with the AMC-I structure but was almost identical to that of Na5min with the
197 AMC-II structure. Subsequently, the AMC-II remained unchanged for three days. The
198 characteristic feature of AMC-II is that the third peak of AMC-I was split, and a new peak emerged
199 between the third and fourth peaks. Since the AMC-II structure was also observed during the
200 growth process in Na_2CO_3 solution, these peak changes do not imply that new Rb–O bonds were
201 formed within the AMC-II structure. The AMC-II essentially consisted of a short-range ordered
202 structure formed with Mg and carbonate ions and water molecules. In Rb5min, a small shoulder
203 and peak split were observed at 2.7 Å and 4.2 Å (Fig. 3b). Rb5min might be distinguishable from
204 Rb0min owing to the presence of these spectral features, but this may be considered as a limitation
205 of this study. In the present study, we classified the spectral features into two types: AMC-I
206 immediately after precipitation and AMC-II immediately before crystallization. This classification
207 method is very useful in interpreting the structural transformation from AMC to NSQ. The
208 schematic graphs of Gibbs free energy and equilibrium are shown in Fig. 4. In Na_2CO_3 solution,
209 AMC-I transforms to AMC-II and then crystallizes into NSQ by stirring the solution (Fig. 4a).
210 This continuous structural change that the structure of the AMC transforming into NSQ appears
211 to be a common phenomenon. On the other hand, in Rb_2CO_3 solution, AMC-II does not crystallize
212 into NSQ because the energy barrier between AMC-II and NSQ becomes significantly high. The
213 AMC-II can never cross the energy barrier in Rb_2CO_3 solution (Fig. 4b). That is, in Rb_2CO_3
214 solution, AMC-II is regarded to be in the equilibrium state (metastable phase) with energetic local
215 minima. This result may support the evidence of polyamorphism, which implies the existence of

two (or more) different forms of amorphous materials. It is known that ACCs have an intrinsic structure corresponding to the crystalline polymorphs of calcite and vaterite (Gebauer et al. 2010).

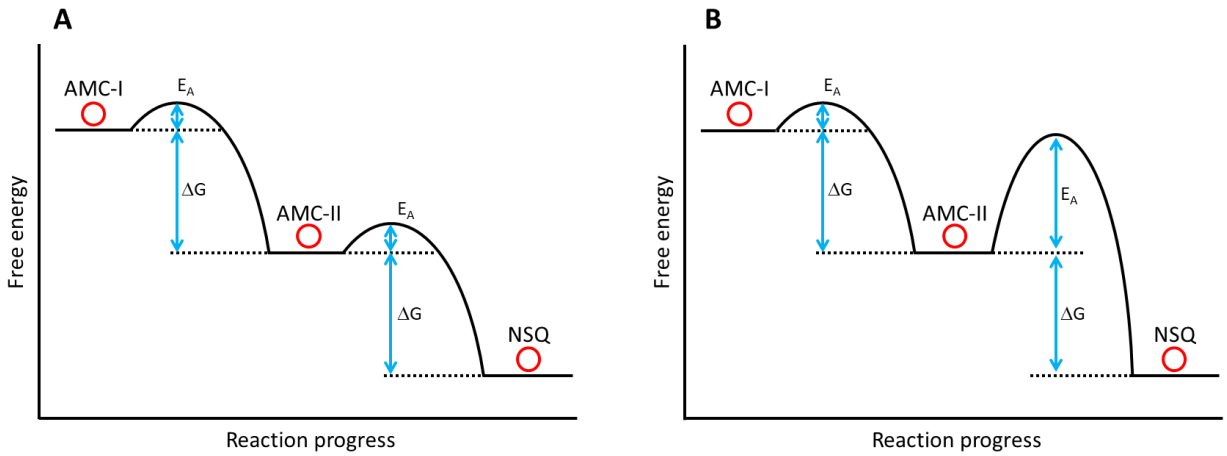

Fig. 4 Schematic graphs of Gibbs free energy and equilibrium in the system. Equilibrium states in (a) Na_2CO_3 solution and (b) Rb_2CO_3 solution

When Na0min was formed in Na_2CO_3 solution, the clusters of AMC-I were comprised of short-range order structures of less than 5 Å size (Fig. 3a). There is a possibility that Na cations were adsorbed on the clusters or incorporated in the amorphous aggregates (Fig. 5a). Subsequently, Na cations were eliminated during crystallization to NSQ (Fig. 5c). In other words, all Na cations must be eliminated during the rearrangement of short-range ordered structure into a long-range periodic ordered structure. However, it can be considered that Rb cations were not eliminated and continued to remain in the AMC-II (Fig. 5b), thereby inhibiting the progress of crystallization into NSQ. This may be the reason why the crystallization process stopped at the AMC-II in Rb_2CO_3 solution.

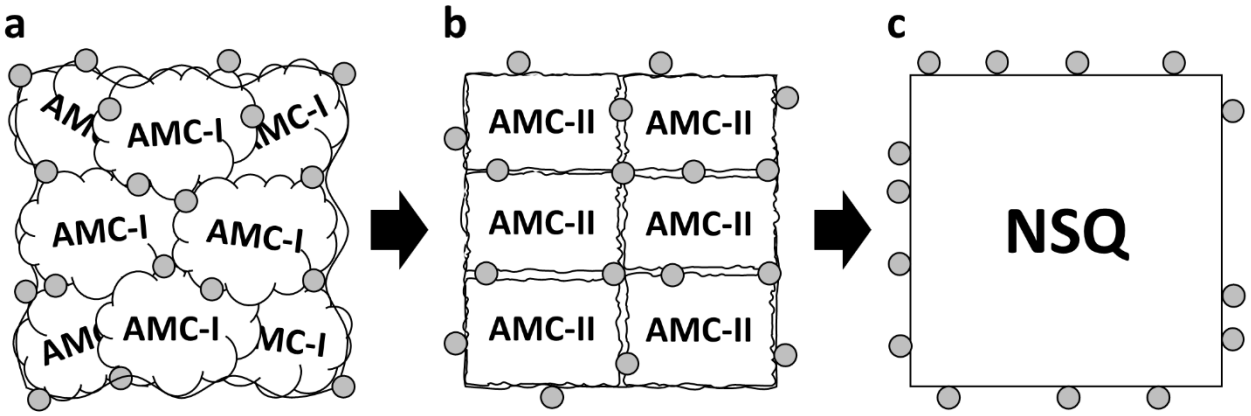

Fig. 5 Schematic images of transformation from AMC-I to NSQ via AMC-II in the alkali carbonate solutions. Gray circles indicate alkali cations adsorbed on the clusters or incorporated in the amorphous aggregates

AMC precipitated immediately after mixing $MgCl_2$ and Na_2CO_3 solutions, resulting in an AMC with an HMG-like structure (AMC-I) (Yamamoto et al. 2021c), which immediately transformed into AMC-II before crystallizing into NSQ. The atom–pair correlation peaks above 5 Å in Rb0min were stronger than those in Na0min. That is, AMC-I is the first structure to form when Mg^+ and CO_3^- ions associate as nucleation clusters, whereas AMC-II structure forms before NSQ crystallization. The structure of AMC-II did not correlate with either the HMG or the NSQ structures (Fig. 6). This suggests that AMC-II probably has an intermediate structure between HMG and NSQ structures.

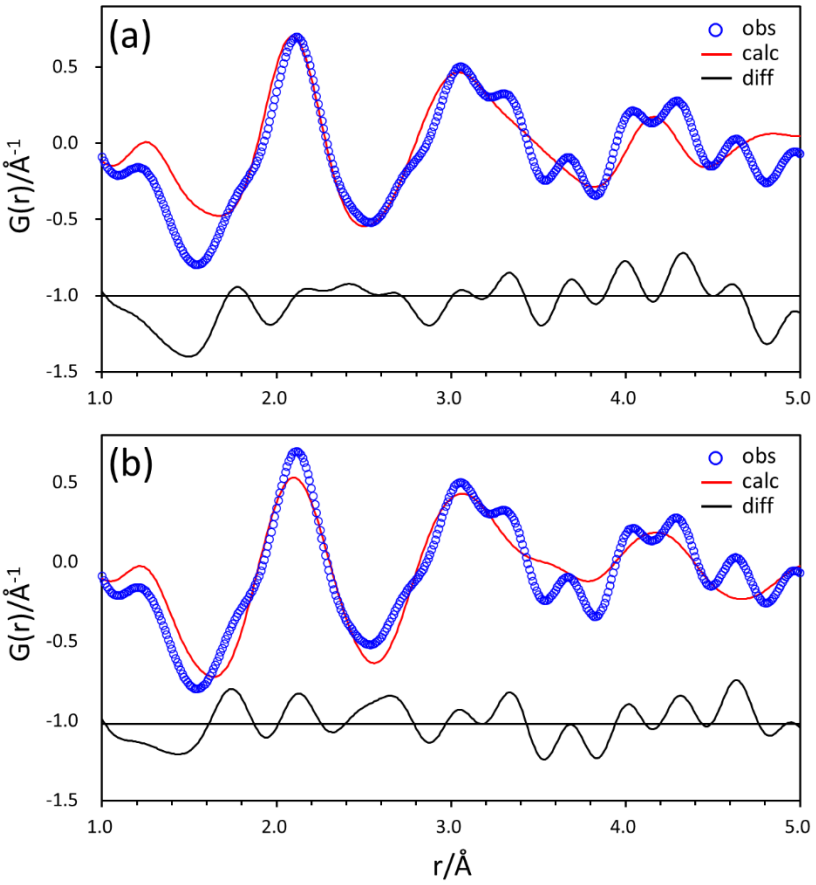

246

247 **Fig. 6** Pair distribution function fitting result of Rb3day with (a) hydromagnesite structure (Akao
248 and Iwai 1977) and (b) nesquehonite structure (Giester et al. 2000)

249

250 The atom–pair correlations between 1.0 Å and 4.5 Å in Cs0min and Na0min exhibited similar
251 peak patterns (Fig. 3c), suggesting that Cs0min has an AMC-I structure. However, the peaks of
252 Cs0min above 5 Å were stronger than those of Na0min. After stirring for 5 min, the third peak
253 located at ~3.1 Å was slightly split, and a new peak appeared between the third and fourth peaks.
254 This peak pattern is characteristic of the AMC-II structure. The split peaks between 3.0 Å and 3.5
255 Å of Cs5min subsequently merged into a broad peak in Cs10min. As mentioned previously,
256 Cs10min exhibited slight diffraction peaks corresponding to NSQ. Therefore, this change in peak
257 pattern from Cs5min to Cs10min indicates the beginning of crystallization of NSQ from AMC-II.

NSQ does not crystallize directly from AMC-I but goes through the AMC-II phase. The split peaks at 4.2 Å merged into a single broad peak after three days. As a result, the peaks between 1.0 Å and 4.5 Å became almost similar to the characteristic four peaks of AMC-I with the HMG-like structure. Considering that NSQ transforms into DYP, which has an HMG-type structure, through a solvent-mediated process (Tanaka et al., 2019), it dissolves and transforms into AMC-I after three days. Although we could not confirm whether the AMC-II structure appeared during dissolution, the $MgCO_3$ hydrate in Cs3day might have crystallized into DYP.

Thermal decomposition process of NSQ

Fig. 7a shows the variations in the XRD pattern of Na10min (NSQ) as a function of heating temperature, which is in good agreement with the previous experimental results (Ballirano et al., 2010; Jauffret et al., 2015). During thermal decomposition, NSQ loses a water molecule above 100 ºC, resulting in the partial collapse of NSQ structure and the formation of a crystalline phase "phase X" (approximately $MgCO_3 \cdot 2H_2O$) (Jauffret et al. 2015). Upon further heating, phase X converts into an amorphous phase above 200 ºC. Periclase (MgO) appears above 400 ºC after $MgO \cdot 2MgCO_3$ crystallizes around 300 ºC. Jauffret et al. (2015) described the regeneration of NSQ upon rehydration of either phase X or the amorphous phase. This suggests that sufficient structural elements persist throughout the initial stages of decomposition to reconstitute NSQ. Fig. 7b exhibits the temperature variations in PDF patterns of NSQ. The atom–pair correlations observed between 200 and 250 ºC were reduced above 5 Å due to the lack of long-range periodicity. As suggested by Jauffret et al. (2015), the fundamental local structure of NSQ was maintained during the heating process. The spectral features of the amorphous phase observed at 250 ºC were similar to that of AMC-I, which possessed the first and second peaks at 1.3 Å and 2.1 Å and the third and

fourth peaks at 3.1 Å and 4.2 Å, respectively. The AMC-II, however, was characterized by a peak split on the third and/or the fourth peak and a new peak appearing between the third and fourth peaks. Since a peak is observed between the third and fourth peaks in the PDF pattern at 200 ºC, this amorphous phase may have the structural features of AMC-II. Thus, the AMC appearing in the thermal decomposition processes has essentially the same structure as that formed in the nucleation and crystallization processes.

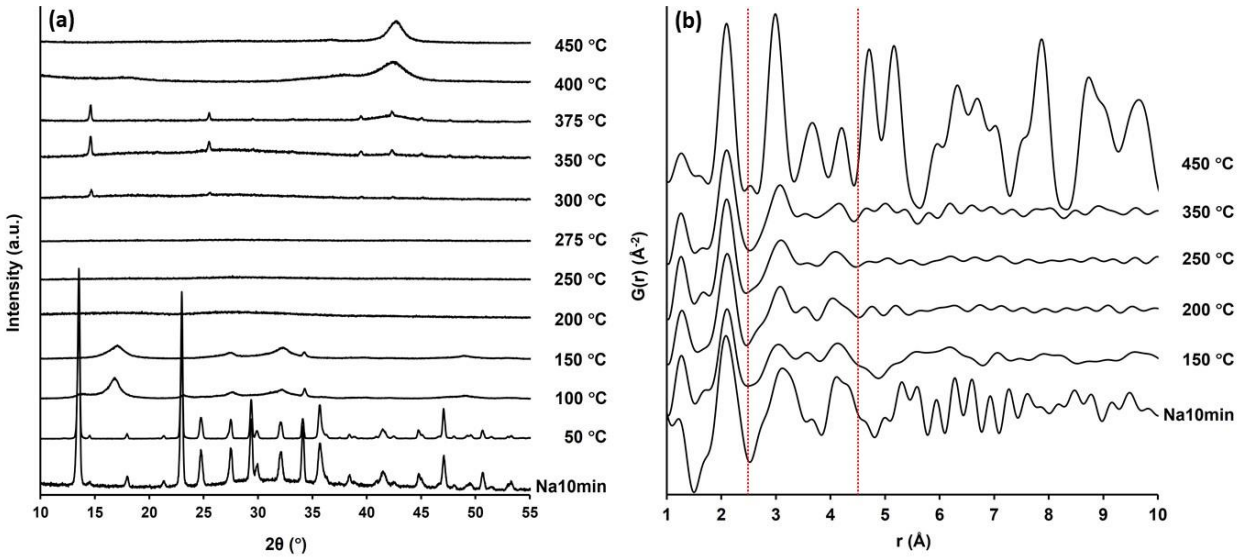

Fig. 7 Thermal variations in (a) X-ray diffraction and (b) pair distribution function patterns of Na10min

Conclusions

This paper reports the structural variations of magnesium carbonate hydrates during nucleation, crystallization, and thermal decomposition processes. These were investigated using XRD and atomic PDF methods. AMC was formed immediately after mixing $MgCl_2$ and alkali carbonate solutions. Two different structures were observed in AMC: one formed immediately after mixing

297 $MgCl_2$ and Na_2CO_3 or Cs_2CO_3 solutions (AMC-I) and the other appeared before crystallization to
298 NSQ (AMC-II). Additionally, AMC-II also appeared when Rb_2CO_3 was used as a carbonate source.
299 AMC-I crystallized into NSQ via AMC-II, suggesting that AMC-II was intermediate to the HMG
300 and NSQ structures. The amorphous phase occurring during the thermal decomposition possessed
301 the AMC-I structure. Thus, despite the limitations of the experimental results, this study provides
302 evidence for the existence of polyamorphism in the AMCs. Further research is needed to fully
303 understand the behavior and fate of AMC during the crystallization and decomposition of
304 magnesium carbonate hydrates.
305
306
307 **Acknowledgments**
308 The authors would like to thank two anonymous reviewers for their constructive comments that
309 helped improve the manuscript. PDF measurements performed at BL22XU of SPring-8 were
310 approved by the Photon Factory Program Advisory Committee (Proposal No. 2021A3737). This
311 work was supported by JSPS KAKENHI Ggrant number JP20K04124).
312
313 **Funding**
314 This work was supported by KAKENHI (Grant number JP20K04124) granted to Atsushi Kyono.
315
316 **Declaration of interests**
317 The authors declare that they have no known competing financial interests or personal
318 relationships that could have appeared to influence the work reported in this paper.
319

Ethics approval

Not applicable

Consent

Not applicable

Authors' contribution statement

G. Yamamoto: Sample preparation, Synchrotron X-ray measurement, Data analysis, and Writing; A. Kyono: Supervision, Synchrotron X-ray measurement, Data analysis, Funding acquisition, and Writing – review and editing; S. Okada: Synchrotron X-ray measurement; All authors reviewed and approved the manuscript.

References

Akao M, Iwai S (1977) The hydrogen bonding of hydromagnesite. Acta Crystallogr B Struct Crystallogr Cryst Chem 33:1273–1275. https://doi.org/10.1107/S0567740877005834.

Aminu MD, Nabavi, SA, Rochelle CA, Manovic V (2017) A review of developments in carbon dioxide storage. Appl Energy 208:1389–1419. https://doi.org/10.1016/j.apenergy.2017.09.015.

Bachu S, Gunter WD, Perkins, EH (1994) Aquifer disposal of CO_2: hydrodynamic and mineral trapping. Energy Convers. Manag 35:269–279. https://doi.org/10.1016/0196-8904(94)90060-4.

Back ME, Mandarino JA (2008) Fleischer's Glossary of Mineral Species. Mineralogical Record Inc., Tucson.

Ballirano P, De Vito C, Ferrini V, Mignardi S (2010) The thermal behaviour and structural stability of nesquehonite, $MgCO_3 \cdot 3H_2O$, evaluated by in situ laboratory parallel-beam X-ray powder diffraction: new constraints on CO_2 sequestration within minerals. J Hazard Mater 178:522–528. https://doi.org/10.1016/j.jhazmat.2010.01.113.

Ballirano P, De Vito C, Mignardi S, Ferrini V (2013) Phase transitions in the $MgCO_2H_2O$ system and the thermal decomposition of dypingite, $Mg_5(CO_3)_4(OH)_2 \cdot 5H_2O$: implications for geosequestration of carbon dioxide. Chem Geol 340:59–67. https://doi.org/10.1016/j.chemgeo.2012.12.005.

Beinlich A, Austrheim H (2012) In situ sequestration of atmospheric CO_2 at low temperature and surface cracking of serpentinized peridotite in mine shafts. Chem Geol 332–333, 32–44. https://doi.org/10.1016/j.chemgeo.2012.09.015.

Bhattacharjya D, Selvamani T, Mukhopadhyay I (2012) Thermal decomposition of hydromagnesite. J Therm Anal Calorim 107:439–445. https://doi.org/10.1007/s10973-011-1656-9.

DECC (2012) CCS Road Map - Supporting Deployment of Carbon Capture and Storage in the UK.

Di Lorenzo F, Rodríguez-Galán RM, Prieto M (2014) Kinetics of the solvent-mediated transformation of hydromagnesite into magnesite at different temperatures. Mineral Mag 78:1363–1372. https://doi.org/10.1180/minmag.2014.078.6.02.

Farrow CL, Juhas P, Liu JW, Bryndin D, Božin ES, Bloch J, Proffen T, Billinge SJL (2007) PDFfit2 and PDFgui: computer programs for studying nanostructure in crystals. J Phys Condens Matter 19:335219. https://doi.org/10.1088/0953-8984/19/33/335219.

364 Frost RL, Bahfenne S, Graham J, Reddy BJ (2008) The structure of selected magnesium carbonate
365 minerals - A near infrared and mid-infrared spectroscopic study. Polyhedron 27:2069–
366 2076. https://doi.org/10.1016/j.poly.2008.03.019.
367 Gebauer D, Gunawidjaja PN, Ko JYP, Bacsik Z, Aziz B, Liu LJ, Hu YF, Bergström L, Tai CW,
368 Sham TK, Edén M, Hedin N (2010) Proto-calcite and proto-vaterite in amorphous calcium
369 carbonates. Angew Chem Int Ed Engl 49:8889–8891.
370 https://doi.org/10.1002/anie.201003220.
371 Giester G, Lengauer CL, Rieck B (2000) The crystal structure of nesquehonite, $MgCO_3 \cdot 3H_2O$,
372 from Lavrion, Greece. Mineral Petrol 70:153–163. https://doi.org/10.1007/s007100070001.
373 Hänchen M, Prigiobbe V, Baciocchi R, Mazzotti M (2008) Precipitation in the Mg-carbonate
374 system - effects of temperature and CO_2 pressure. Chem Eng Sci 63:1012–1028.
375 https://doi.org/10.1016/j.ces.2007.09.052.
376 Hopkinson L, Kristova P, Rut, K, Cressey G (2012) Phase transitions in the system MgO-CO_2-
377 H_2O during CO_2 degassing of Mg-bearing solutions. Geochim Cosmochim Acta 76:1–13.
378 https://doi.org/10.1016/j.gca.2011.10.023.
379 Hunt JM (1972) Distribution of carbon in crust of earth. Am Assoc Petrol Geol Bull 56:2273–
380 2277.
381 Jauffret G, Morrison J, Glasser FP (2015) On the thermal decomposition of nesquehonite. J Therm
382 Anal Calorim 122:601–609. https://doi.org/10.1007/s10973-015-4756-0.
383 Jensen ACS, Imberti S, Habraken WJEM, Bertinetti L (2020). Small ionic radius limits magnesium
384 water interaction in amorphous calcium/magnesium carbonates. J Phys Chem C 124:6141–
385 6144. https://doi.org/10.1021/acs.jpcc.9b11594.

Kloprogge JT, Martens WN, Nothdurft L, Duong LV, Webb GE (2003) Low temperature synthesis and characterization of nesquehonite. J Mater Sci Lett 22:825–829. https://doi.org/10.1023/A:1023916326626.

Kristova P, Hopkinson LJ, Rutt KJ, Hunter HMA, Cressey G (2014) Carbonate mineral paragenesis and reaction kinetics in the system MgO-CaO-CO_2-H_2O in presence of chloride or nitrate ions at near surface ambient temperatures. Appl Geochem 50:16–24. https://doi.org/10.1016/j.apgeochem.2014.08.005.

Oelkers EH, Gislason SR, Matter J (2008) Mineral carbonation of CO_2. Elements 4:333–337. https://doi.org/10.2113/gselements.4.5.333.

Perchiazzi N, Merlino S (2006) The malachite–rosasite group: crystal structures of glaukosphaerite and pokrovskite. Eur J Mineral 18:787–792. https://doi.org/10.1127/0935-1221/2006/0018-0787.

Qiu X, Thompson JW, Billinge SJL (2004) PDFgetX2: a GUI-driven program to obtain the pair distribution function from X-ray powder diffraction data. J Appl Crystallogr 37:678. https://doi.org/10.1107/S0021889804011744.

Radha AV, Fernandez-Martinez A, Hu YD, Jun YS, Waychunas GA, Navrotsky A (2012) Energetic and structural studies of amorphous $Ca_{1-x}Mg_xCO_3 \cdot nH_2O$ ($0 \leq x \leq 1$). Geochim Cosmochim Act. 90:83–95. https://doi.org/10.1016/j.gca.2012.04.056.

Reeder RJ (1983) Crystal chemistry of the rhombohedral carbonates, in: Reeder, R.J. (Ed.), Carbonates: Mineralogy and Chemistry. Rev Mineral 11. Mineralogical Communications Society of America, Washington, District of Columbia pp. 1–47.

Ren HR, Chen Z, Wu YL, Yang MD, Chen J, Hu HS, Liu J (2014) Thermal characterization and kinetic analysis of nesquehonite, hydromagnesite, and brucite, using TG-DTG and DSC

techniques. J Therm Anal Calorim 115:1949–1960. https://doi.org/10.1007/s10973-013-3372-0.

Rodriguez-Blanco JD, Shaw S, Benning LG (2011) The kinetics and mechanisms of amorphous calcium carbonate (ACC) crystallization to calcite, via vaterite. Nanoscale 3:265–271. https://doi.org/10.1039/c0nr00589d.

Sanna A, Uibu M, Caramanna G, Kuusik R, Maroto-Valer MM (2014) A review of mineral carbonation technologies to sequester CO_2. Chem Soc Rev 43:8049–8080. https://doi.org/10.1039/c4cs00035h.

Seto Y, Nishio-Hamane D, Nagai T, Sata N (2010) Development of a software suite on X-ray diffraction experiments. Rev High Press Sci Technol 20:269–276. https://doi.org/10.4131/jshpreview.20.269.

Tanaka J, Kawano J, Nagai T, Teng H (2019) Transformation process of amorphous magnesium carbonate in aqueous solution. J Mineral Petrol Sci 114:105–109. https://doi.org/10.2465/jmps.181119b.

Tobler DJ, Rodriguez Blanco JD, Sørensen HO, Stipp SLS, Dideriksen K (2016) Effect of pH on amorphous calcium carbonate structure and transformation. Cryst Growth Des 16:4500–4508. https://doi.org/10.1021/acs.cgd.6b00630.

Wang Y, Li ZB, Demopoulos GP (2008) Controlled precipitation of nesquehonite ($MgCO_3 \cdot 3H_2O$) by the reaction of $MgCl_2$ with $(NH_4)_2CO_3$. J Cryst Growth 310:1220–1227. https://doi.org/10.1016/j.jcrysgro.2008.01.002.

White CE, Henson NJ, Daemen LL, Hartl M, Page K (2014) Uncovering the true atomic structure of disordered materials: the structure of a hydrated amorphous magnesium carbonate ($MgCO_3 \cdot 3D_2O$). Chem Mater 26:2693–2702. https://doi.org/10.1021/cm500470g.

Yamamoto G, Kyono A, Abe J, Sano-Furukawa A, Hattori T (2021b) Crystal structure of nesquehonite, $MgCO_3 \cdot 3H(D)_2O$ by neutron diffraction and effect of pH on structural formulas of nesquehonite. J Mineral Petrol Sci 116:96–103. https://doi.org/10.2465/jmps.200117.

Yamamoto G, Kyono A, Okada S (2022) Thermal decomposition process of dypingite $Mg_5(CO_3)_4(OH)_2 \cdot 5H_2O$. Mater Lett 308. https://doi.org/10.1016/j.matlet.2021.131125, 131125.

Yamamoto G, Kyono A, Sano Y, Matsushita Y, Yoneda Y (2021a) In situ and ex situ studies on thermal decomposition process of hydromagnesite $Mg_5(CO_3)_4(OH)_2 \cdot 4H_2O$. J Therm Anal Calorim 144:599–609. https://doi.org/10.1007/s10973-020-09618-7.

Yamamoto G., Kyono A, Okada S (2021c) Temperature dependence of amorphous magnesium carbonate structure studied by PDF and XAFS analyses. Sci Rep 11:22876. https://doi.org/10.1038/s41598-021-02261-8.

Zhang ZP, Zheng YJ, Ni YW, Liu ZM, Chen JP, Liang XM (2006) Temperature- and pH-dependent morphology and FT-IR analysis of magnesium carbonate hydrates. J Phys Chem B. 110:12969–12973. https://doi.org/10.1021/jp061261j.